Available online at www.sciencedirect.com
ScienceDirect
Microporous and Mesoporous Materials 112 (2008) 14–25
MICROPOROUS AND MESOPOROUS MATERIALS
www.elsevier.com/locate/micromeso

Synthesis and catalytic properties of manganese(II) and oxovanadium(IV) complexes anchored to mesoporous MCM-41

Tiago A. Fernandes [a], Carla D. Nunes [a], Pedro D. Vaz [a], Maria José Calhorda [a], Paula Brandão [b], João Rocha [b], Isabel S. Gonçalves [b], Anabela A. Valente [b], Liliana P. Ferreira [c,d], Margarida Godinho [c], Paula Ferreira [e,*]

[a] Department of Chemistry and Biochemistry, CQB, Faculty of Sciences of the University of Lisbon, Campo Grande, 1749-016 Lisboa, Portugal
[b] Department of Chemistry, CICECO, University of Aveiro, 3810-193 Aveiro, Portugal
[c] CFMC-UL/Department of Physics, Faculty of Science of the University of Lisbon Ed. C8, Campo Grande, 1749-016 Lisboa, Portugal
[d] Department of Physics, Faculty of Sciences and Technology, University of Coimbra, 3004-516 Coimbra, Portugal
[e] Department of Ceramics and Glass Engineering, CICECO, University of Aveiro, 3810-193 Aveiro, Portugal

Received 25 June 2007; received in revised form 4 September 2007; accepted 5 September 2007
Available online 14 September 2007

Abstract

Reaction of $[Mn^{III}(acac)_3]$ and $[V^{IV}O(acac)_2]$ with the 1,4-diazabutadiene (DAB) ligands Ph–DAB–$(CH_2)_3$R [R = Si(OEt)$_3$(**1a**); H (**1b**)] (L) leads to complexes of the type $[Mn^{II}(acac)_2L]$ and $[V^{IV}O(acac)L]Cl$ in good yields. These complexes were characterised by spectroscopic techniques, and magnetic measurements showed that in the case of the manganese the metal was reduced during the reaction with the nitrogen ligand.

The oxovanadium and manganese complexes bearing the ligand with triethoxysilyl groups Ph–DAB–$(CH_2)_3Si(OEt)_3$(**1a**) were immobilised in ordered MCM-41 by carrying out a grafting reaction. Tethered complexes of the same type were prepared by treating MCM-41 first with a toluene solution of **1a** under reflux; manganese(III) and oxovanadium(IV) precursors were then introduced into the MCM-41-ligand by pore volume impregnation of complex solutions. The modified materials were characterised by powder X-ray diffraction, solid-state NMR (^{13}C, ^{29}Si), FTIR, thermogravimetric studies and low temperature nitrogen adsorption isotherms. The grafted materials contained 0.7 wt% Mn and 0.8 wt% V, while higher metal loadings were achieved when the materials were prepared by tethering (2.9 wt% Mn and 2.4 wt% V).

The modified materials are active catalysts for the oxidation of *cis*-cyclooctene using *tert*-butylhydroperoxide as oxygen donor, at 328 K, yielding 1,2-epoxycyclooctane as the main reaction product and 1,2-cyclooctanediol as a by-product. The vanadium-containing materials are more efficient epoxidation catalysts than the manganese ones. The catalytic behaviour of the heterogenised catalysts was also compared with that observed in homogeneous phase for the complexes $[Mn(acac)_2L]$ and [VO(acac)L]Cl. The vanadium catalysts exhibited the highest catalytic activity, whereas the manganese catalysts were the least active and selective to epoxide formation.

Keywords: Mesoporous materials; MCM-41; Manganese; Oxovanadium; Nitrogen ligands; Epoxidation

1. Introduction

Amorphous silica, alumina and other inorganic oxides have their surface covered by hydroxyl groups, which can be easily functionalised by reaction with appropriate molecules, and have thus found widespread applications as supports for species active in a variety of processes [1,2]. Properties such as the high specific surface area, mechanical stability, and promotion of well-dispersed active sites, make these supports interesting [2]. The discovery of ordered mesoporous materials in 1992 led to a resurgence in the area of supported reagents [3,4], with the emergence

* Corresponding author. Tel.: +351 234 370264; fax: +351 234 425300.
E-mail address: pcferreira@ua.pt (P. Ferreira).

1387-1811/$ - see front matter © 2007 Elsevier Inc. All rights reserved.
doi:10.1016/j.micromeso.2007.09.009

of micelle-templated inorganic oxides as promising alternatives [5]. These materials present as additional advantages relative to amorphous silicas, the fact that the ordered mesopores and higher specific surface area may allow higher loadings of supported reagents, improve active site accessibility and allow catalytic reactions to occur in constrained environments (for example, those involving bulky substrate and/or product molecules, in liquid phase) [6]. These materials have been used as hosts for the immobilisation of coordination compounds to be applied in several fields, such as catalysis and photo- or electro-chemistry [7,8]. Several works concerning the derivatisation of hexagonally ordered mesoporous MCM-41 for catalysis purposes can be found in the literature [9,10], offering the advantages of easy recovery and reuse of the catalyst. The application of MCM-41-supported Mo(VI) complexes, prepared by grafting and tethering techniques, as catalysts for olefin epoxidation, has been well documented [11–14]. The use of these host materials to support magnetically active derivatives of first row transition metals has been less investigated.

Compounds of Mn(II/III) and V(IV) play vital and versatile roles in the redox biochemistry of many organisms [15,16]. Manganese is the metal centre in enzymes such as catalase, superoxidase and dismutase, while vanadium plays an important role in haloperoxidases, as well as in nitrogenases, and an increased knowledge of their catalytic activity in oxidation processes can only be advantageous. Porphyrin ligands coordinate several metals, such as Fe, Mn and Ni, providing environments close to the biological ones [15,16]. Simpler bidentate nitrogen donor ligands, as 1,4-diazabutadienes (DAB), are also versatile since their electronic and steric properties may be fine-tuned by changing the nature of the substituent groups.

Both a pure silica and an aluminosilicate MCM-41 were the supports taken by Luan et al. [17] to immobilise 2,2′-bipyridine manganese(II) complexes [MnL_2] using an impregnation technique. The heterogeneous complexes were effective active sites for oxidation–reduction reactions at low temperature. A Mn(III) complex was also reported as having been immobilised onto the surface of MCM-41 [18] by a tethering approach. First, a functionalised ligand was covalently bound to the surface and then the metal species was directly added to this ligand, forming the complex directly inside the mesoporous material. Several complexes of Mo bearing DAB ligands have been successfully immobilised on the surface of ordered mesoporous silicas by grafting or tethering techniques, for application as catalysts for polymerisation reactions [19] and epoxidation of olefins [14].

In the present work, the immobilisation of manganese and vanadium complexes bearing 1,4-diazabutadiene ligands on MCM-41 host materials by grafting and tethering techniques, is described. A comparative study of the final hybrid mesostructured materials obtained by the two techniques was carried out, by means of solid-state techniques and determination of magnetic properties. The unsupported complexes were also synthesised and characterised. The catalytic performance of all prepared materials was investigated in the oxidation of *cis*-cyclooctene with *tert*-butylhydroperoxide (*t*-BuOOH).

2. Experimental section

2.1. Materials and methods

Starting materials were obtained from commercial sources and used as received. All preparations and manipulations were carried out using standard Schlenk techniques under nitrogen. Solvents were dried by standard procedures (toluene, methanol, and diethyl ether with Na/benzophenone ketyl; CH_2Cl_2 with CaH_2), distilled under nitrogen and kept over 4 Å molecular sieves. Elemental analysis was performed at the University of Vigo. Powder X-ray diffraction (PXRD) data was collected on a Phillips PW 1710 diffractometer using Cu–Kα radiation. The thermal studies were performed using a TG–DSC 111 from Setaram at a heating rate of 10 K min^{-1} under nitrogen. ^{29}Si solid-state NMR spectra were recorded at 79.49 MHz, on a (9.4 T) Bruker Avance 400P spectrometer. ^{29}Si MAS NMR spectra were recorded with 40° pulses, a spinning rate of 5.0 kHz, and 60 s recycle delays. ^{29}Si CP MAS NMR spectra were recorded with 4 μs ^1H 90° pulses, 8 ms contact time, a spinning rate of 5 kHz, and 4 s recycle delays. ^{13}C CP MAS NMR spectra were recorded with a 4.5 μs ^1H 90° pulse, 2 ms contact time, a spinning rate of 7 kHz, and 4 s recycle delays. Chemical shifts are quoted in ppm from TMS. ^{13}C CP MAS NMR spectra were also recorded in the solid state at 125.76 MHz on a Bruker Avance 500 spectrometer.

TGA studies were performed using a Perkin–Elmer TGA7 thermobalance system at a heating rate of 10 K min^{-1} under nitrogen. FTIR spectra were measured with a Nicolet 6700 FTIR spectrometer using KBr pellets (for complexes) in transmission mode and also using Diffuse Reflectance (for mesoporous materials). All FTIR spectra were measured using 2 cm^{-1} resolution.

The precursor complexes $Mn(acac)_3$ [20] and $VO(acac)_2$ [21] were prepared as described previously.

Purely siliceous MCM-41 was synthesised as reported using $[(C_{14}H_{29})N(CH_3)_3]Br$ ($C_{14}TMABr$) as the templating agent [6]. Before the grafting experiments with MCM-41, physisorbed water was removed from the calcined material by heating at 453 K in vacuum (10^{-2} Pa) for 2 h. Ph–DAB–$(CH_2)_3R$ [R = $Si(OEt)_3$(**1a**); H (**1b**)] ligands were synthesised by a described procedure [14].

2.2. Preparation of the complexes of the type $[Mn(acac)_2\{Ph–DAB–(CH_2)_3R\}]$ (**2a**, **2b**) and $[VO(acac)\{Ph–DAB–(CH_2)_3R\}]Cl$ (**3a**, **3b**) (R = $Si(OEt)_3$, H)

A solution of the precursor complexes [$Mn(acac)_3$] (0.70 g, 2 mmol) or [$VO(acac)_2$] (0.53 g, 2 mmol) in methanol (10 mL) was treated with 1 equivalent of either ligand

1a and **1b** in methanol (10 mL). HCl 37% (0.2 mL) was added to the resulting solution and stirred under reflux for 3 h under a N_2 atmosphere. The solvent was then evaporated, and the resultant solid product washed with CH_2Cl_2 and dried in vacuum.

2.2.1. [Mn(acac)$_2${Ph–DAB–(CH$_2$)$_3$Si(OEt)$_3$}] (**2a**)

Yield: 1.57 g (90%). Anal. Calcd for $C_{42}H_{66}MnN_2O_{10}Si_2$ (870.10): C, 57.98; H, 7.65; N, 3.22; Mn, 6.31. Found C, 56.44; H, 8.98; N, 3.29; Mn 6.10. IR (KBr, cm^{-1}): 2939 (w), 1684 (w), 1604 (s), 1560 (s), 1536 (vs), 1496 (w), 1449 (m), 1363 (s), 1282 (m), 1213 (m), 1190 (w), 1108 (sh), 1066 (vs), 1025 (vs), 989 (sh), 937 (s), 794 (m), 764 (m), 698 (s), 643 (m). ^{1}H NMR (400 MHz, $CDCl_3$, r.t., TMS): $\delta = 0.75$ (s bd, 4H, $SiCH_2$), 1.38 (m, 18H, OCH_2CH_3), 1.60 (m, 4H, $CH_2CH_2CH_2$), 1.85 (s, 12H, CH_3 acac), 3.05 (s bd, 4H, NCH_2; 12H, OCH_2CH_3; 2H, acac), 7.01–7.27 (m, 6H, Ph), 7.51 (s, 4H, Ph) ppm.

2.2.2. [Mn(acac)$_2${Ph–DAB–(CH$_2$)$_2$CH$_3$}] (**2b**)

Yield: 1.03 g (94%). IR (KBr, cm^{-1}): 3449(vs), 3206(w), 3066 (w), 2979, (w), 2968 (w), 1680 (s), 1661 (s), 1596 (vs), 1525 (s), 1450 (m), 1342 (s), 1213 (vs), 1175 (w), 877 (s), 719 (s), 697 (m), 643 (s). ^{1}H NMR (400 MHz, $CDCl_3$, r.t., TMS): $\delta = 0.87$ (d, 6H, CH_2CH_3), 1.66 (m, 4H, $CH_2CH_2CH_3$), 1.99 (s, 12H, CH_3 acac), 3.36 (s bd, 4H, NCH_2; 2H, acac), 7.23–7.66 (m, 8H, Ph), 7.87–7.95 (m, 2H, Ph) ppm.

2.2.3. [VO(acac){Ph–DAB–(CH$_2$)$_3$Si(OEt)$_3$}]Cl (**3a**)

Yield: 1.39 g (85%). Anal. Calcd for $C_{37}H_{59}ClVN_2O_9Si_2$ (818.45): C, 54.30; H, 7.27; N, 3.42. Found C, 53.88; H, 9.15; N, 3.70. IR (KBr, cm^{-1}): ν 2939 (w), 1684 (w), 1564 (vs), 1526 (s), 1495 (sh), 1448 (w), 1419 (w), 1372 (s), 1358 (s), 1287 (m), 1227 (w), 1190 (w), 1110 (vs), 1070 (vs), 1027 (vs), 995 (vs), 936 (s), 911 (sh), 798 (m), 790 (m), 762 (m), 699 (m), 687 (sh), 595 (w). ^{1}H NMR (400 MHz, $CDCl_3$, r.t., TMS): $\delta = 0.55$ (s bd, 4H, $SiCH_2$), 1.60 (m, 18 H, OCH_2CH_3), 1.60 (m, 4H, $CH_2CH_2CH_2$), 2.70 (s, 12H, CH_3 acac), 3.10 (t, 4H, NCH_2), 4.65 (s bd, 12H, OCH_2CH_3; 2H, acac), 7.2 (m, 4H, Ph), 7.4 (s, 4H, Ph), 7.8 (s, 2H, Ph) ppm.

2.2.4. [VO(acac){Ph–DAB–(CH$_2$)$_2$CH$_3$}]Cl (**3b**)

Yield: 0.88 g (89%). IR (KBr, cm^{-1}): 3425 (vs), 3218 (s), 3068 (s), 2983 (w), 2938 (w), 1679 (vs), 1661 (vs), 1595 (s), 1529 (vs), 1451 (w), 1420 (w),1212 (s), 1175 (w), 1023 (w), 998 (vs), 877 (m), 719 (s), 643 (s), 486 (m). ^{1}H NMR (400 MHz, $CDCl_3$, r.t., TMS): $\delta = 0.79$–0.91 (m, 6H, CH_2CH_3), 1.19 (s, 4H, $CH_2CH_2CH_3$), 1.54 (s, 12H, CH_3 acac), 2.29 (s bd, 4H, NCH_2; 2H, acac), 7.43–7.47 (m, 4H, Ph), 7.59 (t, 2H, Ph), 7.89–7.93 (m, 4H, Ph) ppm.

2.3. Preparation of MCM-41-L (**4**)

A solution of Ph–DAB–(CH$_2$)$_3$Si(OEt)$_3$(**1a**) (0.70 g, 1.13 mmol) in toluene (10 mL) was added to a suspension of MCM-41 (0.8 g) in toluene (10 mL) and the mixture heated at 373 K for 9 h. The resultant solid was then filtered off and washed four times with CH_2Cl_2 (4 × 15 mL), and dried in vacuum at 323 K for 3 h. Elemental analysis found: C, 11.09; N, 1.49; H, 2.71. IR (KBr, cm^{-1}): 3065 (w), 2978 (m), 2932 (w), 1654 (m), 1638 (m), 1622 (m), 1600 (m), 1542 (vw), 1508 (m), 1496 (m), 1450 (m), 1394 (m), 1240 (vs), 1078 (vs), 798 (s), 735 (m), 700 (m). ^{13}C CP MAS NMR: $\delta = 9.1$ ($SiCH_2$), 16.5, 20.8, 23.9, 42.8, 58.0, 127.6 (phenyl-C) ppm. ^{29}Si MAS NMR: $\delta = -53.3$ (bd), −108.6 ppm. ^{29}Si CP MAS NMR: $\delta = -54.3$ (T^1), −59.5 (T^2), −68.7 (T^3), −103.1 (sh, Q^3), −108.7 (sh, Q^4) ppm.

2.4. Preparation of MCM-41/Mn(acac)$_2$[Ph–DAB–(CH$_2$)$_3$Si(OEt)$_3$] (**5**)

A solution of [Mn(acac)$_2${Ph–DAB–(CH$_2$)$_3$Si(OEt)$_3$}] (**2a**) (0.66 g, 0.73 mmol) in methanol (10 mL) was added to a suspension of MCM-41 (1.0 g) in toluene (10 mL) and the mixture stirred at room temperature for 24 h. The solution was then filtered and the pale powder is washed repeatedly with CH_2Cl_2 (4 × 20 mL), before drying in vacuum at room temperature for several hours. Elemental analysis found: C, 16.40; N, 0.90; H, 2.12; Mn, 0.70. IR (KBr, cm^{-1}): 2921 (w), 1605 (m), 1539 (m), 1494 (m), 1452 (m), 1368 (s), 1242 (vs), 1076 (vs), 948 (sh), 804 (s), 732 (m), 695 (m). ^{13}C CP MAS NMR: $\delta = 9.5$, 14.4, 21.1, 26.9, 44.6, 104.7, 127.1 ppm. ^{29}Si MAS NMR: $\delta = -50.5$, −93.5 (Q^2), −103.6 (Q^3), −108.8 (Q^4) ppm.

2.5. Preparation of MCM-41-L/Mn(acac)$_2$ (**5′**)

A solution of [Mn(acac)$_3$] (0.19 g, 0.55 mmol) in methanol (5 mL) was added to a suspension of MCM-41-L (**4**) (0.8 g) in toluene (10 mL) and in the presence of HCl (0.1 mL) and the resulting mixture was stirred overnight at 323 K. The resultant solid was then filtered off and washed with CH_2Cl_2 (4 × 20 mL), and dried in vacuum at room temperature for 3 h. Elemental analysis found: C, 16.8; N, 1.52; H, 2.30; Mn, 2.90. IR (KBr, cm^{-1}): 2930 (vw), 1607 (m), 1570 (m), 1539 (m), 1457 (w), 1362 (m), 1240 (vs), 1081 (vs), 936 (s), 807 (s), 696 (m). ^{13}C CP MAS NMR: $\delta = 10.2$ ($SiCH_2$), 17.2, 20.9, 24.5, 42.8, 57.2, 106.9, 127.8 (phenyl-C), 190.7 (C=O). ^{29}Si MAS NMR: $\delta = -21.9$, −56.0 (bd), −108.5 ppm. ^{29}Si CP MAS NMR: $\delta = -56.5$ (T^1), −59.1 (T^2), −66.1 (T^3), −108.9 (sh, Q^4) ppm.

2.6. Preparation of MCM-41/VO(acac)[Ph–DAB–(CH$_2$)$_3$Si(OEt)$_3$] (**6**)

A solution of [VO(acac){Ph–DAB–(CH$_2$)$_3$Si(OEt)$_3$}]Cl (**3a**) (0.77 g, 0.94 mmol) in methanol (10 mL) was added to a suspension of MCM-41 (0.94 g) in toluene (10 mL) and the mixture stirred at room temperature for 24 h. The solution was then filtered and the pale powder is washed

repeatedly with CH_2Cl_2 (4×20 mL), before drying in vacuum at room temperature for several hours. Elemental analysis found: C, 9.42; N, 1.08; H, 1.55; V, 0.80. IR (KBr, cm^{-1}): 3062 (vw), 2956 (w), 2925 (w), 1633 (m), 1567 (w), 1541(w), 1461 (w), 1366 (w), 1230 (sh), 1240 (vs), 1083 (vs), 949 (sh), 806 (m), 734 (m), 698 (m), 576 (m). ^{13}C CP MAS NMR: $\delta = 11.0$, 16.5, 21.9, 23.8. 42.5, 56.8, 102.7, 128.7 (phenyl-C), 195.9 (C=O) ppm. ^{29}Si MAS NMR: $\delta = -55.6$ (bd), -95.1 (Q^2) -101.1 (Q^3), -108.2 (Q^4) ppm.^{29}Si CP MAS NMR: $\delta = -55.0$ (T^1), -58.4 (T^2), -63.2 (T^3), -92.4 (Q^2), -104.1 (Q^3), -108.5 (Q^4) ppm.

2.7. Preparation of MCM-41-L/VO(acac) (6′)

A solution of $[VO(acac)_2]$ (0.18 g, 0.66 mmol) in methanol (5 mL) was added to a suspension of MCM-41-L (**4**) (0.8 g) in toluene (10 mL) and in the presence of HCl (0.1 mL) and the resulting mixture was stirred overnight at 323 K. The resultant solid was then filtered off and washed with CH_2Cl_2 (4×20 mL), and dried in vacuum at room temperature for 3 h. Elemental analysis found: C, 16.94; N, 1.24; H, 2.27; V, 2.40. IR (KBr, cm^{-1}): 2930 (vw), 1683 (m), 1568 (w), 1538(w), 1450 (vw), 1367 (w), 1241 (vs), 1080 (vs), 936 (s), 800 (m), 733 (m), 696 (m). ^{13}C CP MAS NMR: $\delta = 9.6$ ($SiCH_2$), 21.0, 25.8, 42.8, 58.3, 104.0, 127.9 (phenyl-C), 192.3 (C=O). ^{29}Si MAS NMR: $\delta = -58.9$ (bd), -109.1 ppm. ^{29}Si CP MAS NMR: $\delta = -50.6$ (T^1), -57.7 (T^2), -67.5 (T^3), -98.0, -106.0, -110.3 (sh, Q^4) ppm.

2.8. DFT calculations

DFT [22] calculations were performed using the Gaussian 03 program, rev. B.04 [23]. Molecular structures based on Cambridge Structural Database (CSD) [24] related structures were fully optimised without any symmetry constraints at the unrestricted B3LYP [25] level with the lanl2dz basis set [26] on Mn and V atoms and 6–31 G* basis set [27] for all the remaining atoms. Frequency calculations were performed at the same level to confirm the nature (minima) of the stationary points determined.

2.9. Magnetisation studies

Magnetisation data were collected using a SQUID magnetometer (Quantum Design MPMS) over the temperature range from 2 to 200 K, at applied magnetic fields up to 5.5 T. Besides the paramagnetic signal due to Mn or V ions, a diamagnetic temperature independent contribution was detected in all samples. For each magnetisation versus temperature curve, collected at a certain magnetic field, the diamagnetic fraction was determined from the value of the intercept B in the plot of the magnetic susceptibility χ versus inverse temperature ($\chi = C/T + B$), in the temperature region where the Curie law is valid, and subtracted from the total magnetic signal. The paramagnetic data were then analysed using the spin-Hamiltonian model, providing information on the concentration of metallic ions, their spin, local symmetry and zero-field splitting parameters. Further details on data collection and fitting procedure can be found in [28].

2.10. Catalytic studies

The liquid phase catalytic oxidations were carried out at 328 K under air (atmospheric pressure) in a reaction vessel equipped with a magnetic stirrer and immersed in a thermostated oil bath. 175 mg MCM-41-supported catalyst plus 7.2 mmol cyclooctene (or 1% molar ratio of free complex/substrate) and a substrate/oxidant molar ratio of 0.65 (*tert*-butyl hydroperoxide, 5.5 M in decane) were used. The course of the reaction was monitored using a gas chromatograph (Varian 3800) equipped with a capillary column (SPB-5, $20\ m \times 0.25$ mm) and a flame ionisation detector. The products were identified by gas chromatography–mass spectrometry (HP 5890 Series II GC; HP 5970 Series Mass Selective Detector) using He as carrier gas.

3. Results and discussion

3.1. Synthesis and characterisation of the complexes

The triethoxysilyl ligand Ph–DAB–$(CH_2)_3Si(OEt)_3$ (**1a**) was prepared by the reaction of benzil $[C_6H_5(CO)(CO)C_6H_5]$ with two equivalents of (3-aminopropyl)triethoxysilane [14]. Each of the precursor complexes $[Mn(acac)_3]$ and $[VO(acac)_2]$ (acac = $C_5H_7O_2^-$) was treated in methanol with one equivalent of **1a**, in the presence of HCl, affording, in good yield, two complexes characterised as $[Mn(acac)_2\{Ph–DAB–(CH_2)_3Si(OEt)_3\}]$ (**2a**) and $[VO(acac)\{Ph–DAB–(CH_2)_3Si(OEt)_3\}]Cl$ (**3a**), (Scheme 1).

The FTIR spectra of compounds **2a** and **3a** are dominated by the strong absorptions of the $Si(OEt)_3$ groups, which overlap with other relevant spectral features of the complexes. The coordination of 1,4-diazabutadiene ligand **1a** to the metal centres is supported by the $\nu_{C=N}$ band observed for free **1a** at 1674 cm^{-1} and shifted to 1685 and 1684 cm^{-1} for complexes **2a** and **3a**, respectively. Strong bands assigned to the $\nu_{C=O}$ modes of the acac ligand appear at 1678 and 1660 cm^{-1} for complex **2a**, and at 1565 and 1522 cm^{-1} for complex **3a**. Bands corresponding to the $\nu_{Si–O–Si}$ are observed at 1066 cm^{-1} for complex **2a** and at 1068 cm^{-1} for complex **3a**, indicating some degree of polymerisation. The strong $\nu_{V=O}$ mode shifted from 995 cm^{-1} in the $[VO(acac)_2]$ precursor to 998 cm^{-1} in complex **3a**. The preparation of the analogous ligand Ph–DAB–$(CH_2)_2CH_3$ (**1b**), with terminal methyl groups, instead of the bulky $Si(OEt)_3$ required for surface binding to MCM-41 (Scheme 1), and their complexes $[Mn(acac)_2\{Ph–DAB–(CH_2)_2CH_3\}]$ (**2b**) and $[VO(acac)\{Ph–DAB–(CH_2)_2CH_3\}]Cl$ (**3b**), allowed a better spectroscopic analysis. The $\nu_{C=O}$ bands in **2a** and **3a**, and $\nu_{V=O}$ in **3a**, appear in the same positions in **2b** and **3b**, suggesting that

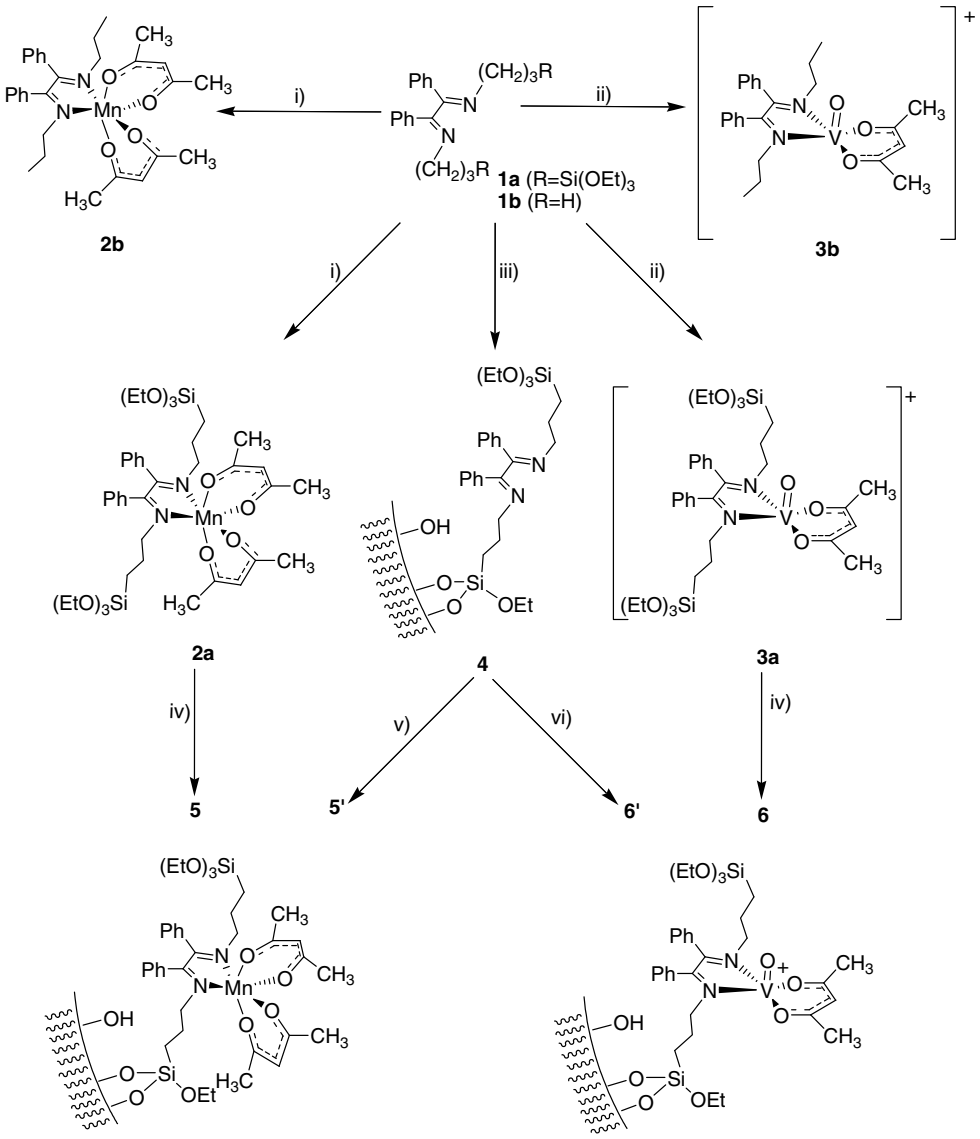

Scheme 1. Schematic overview of the synthetic procedures described in this work. Reagents: (i) $Mn(acac)_3$, MeOH, HCl; (ii) $VO(acac)_2$, MeOH, HCl; (iii) MCM-41, toluene; (iv) MCM-41, toluene, MeOH, HCl; (v) $Mn(acac)_3$, toluene, MeOH, HCl; (vi) $VO(acac)_2$, toluene, MeOH, HCl.

the ligand modification has not led to changes in the coordination environment of the metals.

On the other hand, the bands assigned to the β_{C-H} modes are observed in the range 1600–1400 cm^{-1} for both **2b** and **3b**; ν_{Mn-N} and ν_{Mn-O} modes are observed at 719 and 643 cm^{-1} for complex **2b**, while complex **3b** exhibits the ν_{C-N} mode at 1023 cm^{-1}, the ν_{V-N} modes at 719 cm^{-1} and 643 cm^{-1}, and ν_{V-O} mode at 486 cm^{-1}.

The ^1H and ^{13}C NMR spectra of Ph–DAB–$(CH_2)_3Si(OEt)_3$ (**1a**) agree with those reported [14]. The ^1H NMR spectra of complexes **2a** and **3a** consist of broad signals, consistent with the presence of paramagnetic species, namely V(IV) d^1 and Mn(II) d^5, and are therefore considerably noisy. It was impossible to collect their ^{13}C NMR spectra. The ^1H NMR spectra of both complexes **2a** and **3a** display the signals characteristic of the coordinated ligand **1a**, slightly shifted (Table 1). The CH_3 of the ethyl group is shifted to low field, while the signals of all the other protons in complexes **2a** and **3a** are shifted upfield; there are two signals, assigned to the protons of the acac ligands, at 1.85 and 3.05 ppm (**2a**) or 2.70 and 4.65 (**3a**).

A search in the Cambridge Structural Database [24] did not provide any structures of V(IV) and Mn(II) that could be directly compared with those of **2b** and **3b** (or **2a** and **3a**), and no crystals suitable for a structure determination could be obtained. Therefore, unrestricted DFT calculations [22] were carried out on complexes **2b** and **3b**, using the G03 package [23] at the B3LYP [25] level. The reliability of the computational approach was mainly checked by comparing the calculated vibrational spectra, since there is no structure available with exactly the same coordination sphere around V or Mn. For this comparison, complexes of ligand **1b** were prepared. The calculated structures are shown in Fig. 1.

Table 1
Chemical shifts for the protons of ligand **1a** and complexes **2a** and **3a** (δ/ppm)

Compound	OCH_2CH_3	OCH_2CH_3	CH_2Si	$CH_2CH_2CH_2$	$N{-}CH_2$	Ph	acac
1a	1.15–1.24	3.73–3.84	0.6–0.68	1.76–1.86	3.4–3.44	7.32–7.50 7.57–7.75 7.88–7.93	–
2a	1.38	3.05	0.75	1.60	3.05	7.01–7.27 7.51	1.85 3.05
3a	1.60	4.65	0.55	1.60	3.10	7.20 7.40 7.80	2.70 4.65

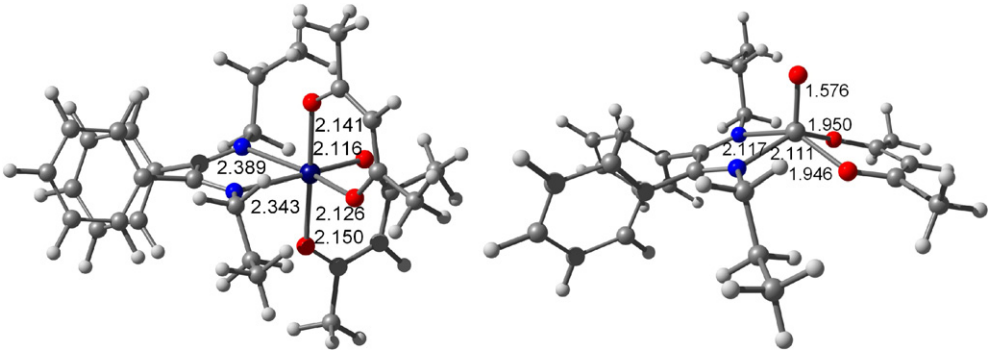

Fig. 1. DFT optimised geometries of complexes $[Mn(acac)_2\{Ph–DAB–(CH_2)_2CH_3\}]$ (**2b**) (left) and $[VO(acac)\{Ph–DAB–(CH_2)_2CH_3\}]^+$ (**3b**) (right), showing some relevant distances.

In $[Mn(acac)_2\{Ph–DAB–(CH_2)_2CH_3\}]$ (**2b**), the formal oxidation state of Mn is II, so that two different spin states are possible, the high spin state S = 5/2 being more stable by 17 kcal mol^{-1}. The octahedral coordination around Mn(II) is distorted by the non equivalence of the ligands, with an O—Mn—O angle of 176°, and two N—Mo—O—O angles of 164° and 162°. The two Mn—O distances to the O trans to the nitrogen donors (2.116 and 2.126 Å) are comparable to 2.117 and 2.124 Å determined in [Mn(acac)(phen)$_2$], the closest Mn(II) complex found, where the acac ligand is also trans to a nitrogen ligand (phen). The other two Mn—O distances are longer (2.141 and 2.150 Å). The Mn—N distances (2.343 and 2.389 Å) are slightly longer than the corresponding distances of 2.279 and 2.321 Å in [Mn(acac)(phen)$_2$].

The V(IV) complexes bearing acac and dinitrogen ligands available in the CSD are hexacoordinate, which makes comparison trickier, but the V=O bond is similar to that found in the structures with REFCODEs XACPLV01, KOBKUH, and KACROV (1.622, 1.588, 1.597 Å). In these complexes, the V—N bonds range from 2.055 to 2.194 Å, very close to 2.111 and 2.117 Å calculated for $[VO(acac)\{Ph–DAB–(CH_2)_2CH_3\}]Cl$ (**3b**), and V—O bonds between 1.971 and 1.989 Å, compared to 1.946 and 1.950 Å in **3b**. For comparison, calculations were also performed on the hexacoordinate $[VO(acac)\{Ph–DAB–(CH_2)_2CH_3\}Cl]$ complex, where vanadium displays a distorted octahedral coordination. The V=O lengthens very slightly to 1.598 Å, the same happening with the V—O (1.982 and 1.977 Å) and V—N (2.143 and 2.147 Å) distances. These bonds lengths are closer to those of the V(IV) complexes used for comparison. Finally, the V—Cl distance is 2.594 Å, indicating a weak bond.

The more characteristic modes, $\nu_{C=N}$ and $\nu_{C=O}$, in the vibrational spectra of **2b** are calculated to appear at 1664 cm^{-1} and 1666 cm^{-1}, for the first, and 1650 cm^{-1} for the later, very close to the observed frequencies of 1680 cm^{-1} ($\nu_{C=N}$), and 1661 cm^{-1} ($\nu_{C=O}$), supporting the formulation proposed for the complex.

The same vibrational modes are calculated for complex **3b** at 1681 cm^{-1}, 1637 cm^{-1} ($\nu_{C=N}$) and 1608 cm^{-1} ($\nu_{C=O}$), which compare with experimental data at 1679 cm^{-1} ($\nu_{C=N}$) and 1661 cm^{-1} ($\nu_{C=O}$). Of relevance is also the $\nu_{V=O}$ mode in **3b** predicted at 1109 cm^{-1} being observed at 998 cm^{-1}. In $[VO(acac)\{Ph–DAB–(CH_2)_2CH_3\}]Cl$ (**3b**), the $\nu_{C=N}$ mode is calculated at 1646 cm^{-1}and the $\nu_{C=O}$ mode at 1640 cm^{-1}.

3.2. Synthesis and characterisation of the functionalised materials

The functionalised materials containing supported complexes were prepared from MCM-41 materials using two different strategies as depicted in Scheme 1.

In the first approach (grafting), treatment of MCM-41 with a solution of $[Mn(acac)_2\{Ph–DAB–(CH_2)_3Si(OEt)_3\}]$

(**2a**) in toluene gave MCM-41/Mn(acac)$_2$[Ph–DAB–(CH$_2$)$_3$Si(OEt)$_3$] (**5**) containing approximately 0.7 wt% Mn (0.12 mmol Mn · g^{-1}). A similar procedure afforded the oxovanadium material MCM-41/VO(acac)[Ph–DAB–(CH$_2$)$_3$Si(OEt)$_3$] (**6**), by incorporating [VO(acac){Ph–DAB–(CH$_2$)$_3$Si(OEt)$_3$}]Cl (**3a**) inside the pores of MCM-41, and led to a content of approximately 0.8 wt% V (0.17 mmol V · g^{-1}).

The second approach consisted of a stepwise construction of the final materials MCM-41-L/Mn(acac)$_2$ (**5′**) and MCM-41-L/VO(acac) (**6′**) by a tethering procedure (Scheme 1). The MCM-41 host material was first treated with a toluene solution of Ph–DAB–(CH$_2$)$_3$Si(OEt)$_3$(**1a**) under reflux for 9 h, leading to the derivatised material MCM-41-L (**4**). The precursor complexes [Mn(acac)$_3$] and [VO(acac)$_2$] were subsequently introduced by pore volume impregnation of toluene/methanol solutions, in the presence of HCl, to give **5′**, with approximately 2.9 wt% Mn (0.52 mmol Mn · g^{-1}), and **6′**, with approximately 2.4 wt% V (0.46 mmol V · g^{-1}), as indicated by elemental analysis.

The powder XRD patterns of the pristine calcined MCM-41 starting material agree with reported patterns, indicating well-ordered materials (Fig. 2) [3,4,29]. Several distinct Bragg peaks are observed in the range $2\theta = 2$–8°, which can be indexed to *hkl* reflections for a hexagonal unit cell (using the strongest reflection, d_{100}, $a = 2d_{100}/\sqrt{3} = 34.0$ Å). Direct grafting of complexes **2a** and **3a** resulted in a reduction of the intensity of the diffraction peaks in materials **5** and **6**, but several distinct Bragg peaks are still observed, indicating retention of the long-range hexagonal symmetry. The attenuation of the peak intensities should not be interpreted as a loss of order, but to a likely reduction in the X-ray scattering contrast between the silica walls and pore-filling material [30]. On the other hand, grafting of the MCM-41 host material with the triethoxysilyl ligand **1a** results in a strong reduction of the intensity of the X-ray diffractions (Fig. 2). Reaction of the MCM-41-L (**4**) with the complexes [Mn(acac)$_3$] or [VO(acac)$_2$] further reduces the intensity of the peaks. The tethering method allows an introduction of a very high content of diazabutadiene ligand, with a consequent reduction of the scattering contrast, and the loading of the metal complexes leads to a further decrease. The peak intensity reduction is less significant in **5** and **6** than in **5′** and **6′** because of the lower ligand and metals contents in the first two. The material **5** is prepared by pore volume impregnation of the metal complex bearing the diazabutadiene ligand. The complex is far bulkier than ligand **1a** and thus may have increased difficulty towards diffusion inside the material pores. The resulting material has thus a much smaller amount of metal than material **5′**, which was prepared by a stepwise approach. Similar results were found for materials **6** and **6′**.

The FTIR spectra of the parent host material MCM-41 is similar to that of other mesoporous silicious matrices. The bands at 1235 cm^{-1} and 1087 cm^{-1} are assigned to

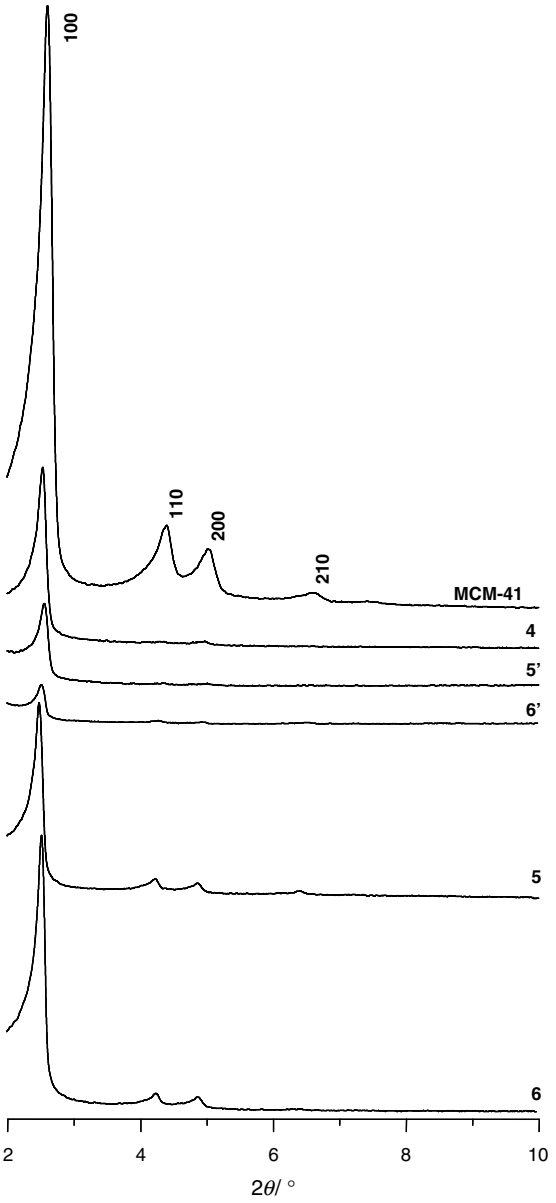

Fig. 2. Powder XRD patterns of MCM-41, MCM-41-L (**4**), MCM-41-L/Mn(acac)$_2$ (**5′**), MCM-41-L/VO(acac) (**6′**), MCM-41/Mn(acac)$_2$[Ph–DAB–(CH$_2$)$_3$Si(OEt)$_3$] (**5**), and MCM-41/VO(acac)[Ph–DAB–(CH$_2$)$_3$Si(OEt)$_3$] (**6**).

the $\nu_{asymSi—O—Si}$ mode of the framework, with the corresponding ν_{sym} mode appearing at ca. 800 cm^{-1}. An absorption at 963 cm^{-1} is assigned to a $\delta_{Si—O}$ mode of the Si—OH groups. The treatment of the MCM with ligand **1a** led to derivatised material MCM-41-L (**4**), which exhibits bands at 3090, 2980, 2950 and 2920 cm^{-1}, assigned to $\nu_{C—H}$ modes of the ligand, and the band at 1678 cm^{-1} to the $\nu_{C=N}$ mode of the ligand. This result suggests that the ligand is indeed immobilised inside the pores of the host material, as previously described [14,19]. In material **4**, it is still possible to assign a very strong band at 1090 cm^{-1} to the $\nu_{asymSi—O—Si}$ mode of the framework, the corresponding ν_{sym} mode appearing at ca. 817 cm^{-1}.

Reaction of **4** with the precursor complexes [Mn(acac)$_3$] and [VO(acac)$_2$] led to the new materials **5′** and **6′**, respectively. It is possible to assign, in the FTIR spectrum of the Mn-containing material **5′**, the band due to the $\nu_{C=N}$ mode of the ligand **1a** at 1675 cm^{-1}, as well as the three bands at 1624 ($\nu_{C=O}$), 1567 (β_{C-H}) and 1538 cm^{-1} ($\nu_{C=C}$) associated with the acac ligand (not shown). The corresponding bands are observed, for material **6′**, at 1683 cm^{-1} ($\nu_{C=N}$) and 1653($\nu_{C=O}$), 1623 (β_{C-H}) and 1559 cm^{-1} ($\nu_{C=C}$) for **1a** and the acac ligand, respectively. The ν_{asym} mode of the Si—O—Si vibration appears at 1078 cm^{-1} in **5′** and 1062 cm^{-1} in **6′**, and the ν_{sym} mode at 809 and 804 cm^{-1}. The $\nu_{V=O}$ is expected to appear at ca. 998 cm^{-1} for material **6′**, as described above for complexes **3a** and **3b**. Indeed, there is a small shoulder at this position, but given its weakness, compared with the intensity of the $\nu_{asymSi-O-Si}$ mode of the framework, the identification remains ambiguous.

For the two materials **5** and **6**, the lower amounts of complex combined with the strong bands of the silica framework prevents a detailed assignment of the vibrational spectra, compared to materials **5′** and **6′**. The $\nu_{C=N}$ of the ligand **1a** is observed at 1678 cm^{-1} and 1682 cm^{-1} in materials **5** and **6**, while the band assigned to the $\nu_{C=O}$ mode of the acac ligand appears at 1630 and 1628 cm^{-1} for **5** or **6**, respectively. The ν_{asym} mode of the framework Si—O—Si units appears at the same positions as those found for the **5′** and **6′** materials. Nevertheless, the presence of the most characteristic bands of the two ligands ($\nu_{C=O}$ and $\nu_{C=N}$, for **1a** and acac) support the coordination of the metal complexes to the pendant ligands **1a** bound to the surface.

Thermogravimetric analyses of the materials **5**, **5′**, **6**, **6′**, and MCM-41-L (**4**) were carried out. Excluding the mass losses due to water up to ca. 393 K, materials **5** and **6** show smaller mass losses (15% and 16%, respectively), than those found for materials **5′** and **6′** (30% and 28%, respectively) above 393 K. As expected, this is in good agreement with results from elemental analysis since the later materials were found to have higher ligand and metal loadings than the former. In addition, materials **5′** and **6′**, prepared by the tethering approach, show higher mass losses than material **4** (mass loss of 20% above 393 K). This is indicative that the metallic fragments were successfully introduced inside the mesopores with the formation of the immobilised complexes as shown in Scheme 1.

The MCM-41 starting material showed type IV N_2 adsorption isotherm, typical of mesoporous solids, according to IUPAC classification [31]. The specific surface area (S_{BET}) and total pore volume (V_P) of pristine MCM-41 are 1046 m^2 g^{-1} and 0.87 cm^3 g^{-1}, respectively (Table 2), and were calculated according with literature data [29,32]. Similar results were obtained for the V-containing materials (**6** and **6′**). The isotherms of the modified materials obtained by grafting (5 and 6) showed a lower N_2 uptake, pointing to a decrease in the specific surface area (28% for **5** and 22% for material **6**). The height of the capillary condensation step and the p/p^0 coordinate of the inflection point decreased significantly, indicating changes in the pore size distribution, owing to grafting of the internal surface of MCM-41 with the manganese and oxovanadium species, **2a** and **3a**, respectively. These effects are even more pronounced in the solids prepared by tethering. Reduction in the S_{BET} and V_P of 57% and 68%, respectively, are already observed after grafting of the ligand **1a**, and S_{BET} and V_P further decreased after the inclusion of the metal complexes. In the case of **5′** and **6′**, S_{BET} and V_P decreased ca. 80% relative to the parent MCM-41 material (Table 2). These results, together with the powder XRD results,

Table 2
Texture parameters taken from N_2 adsorption data collected at 77 K

Sample	S_{BET} (m^{2}g^{-1})[a]	ΔS_{BET} (%)[a]	V_p(cm^{3}g^{-1})	ΔV_p (%)[b]
MCM-41	1046	–	0.87	–
5	744	−28	0.46	−47
6	821	−22	0.45	−48
4	446	−57	0.28	−68
5′	199	−81	0.14	−83
6′	211	−79	0.16	−82

[a] Variation of surface area in relation to parent MCM-41 material.
[b] Variation of total pore volume in relation to parent MCM-41 material.

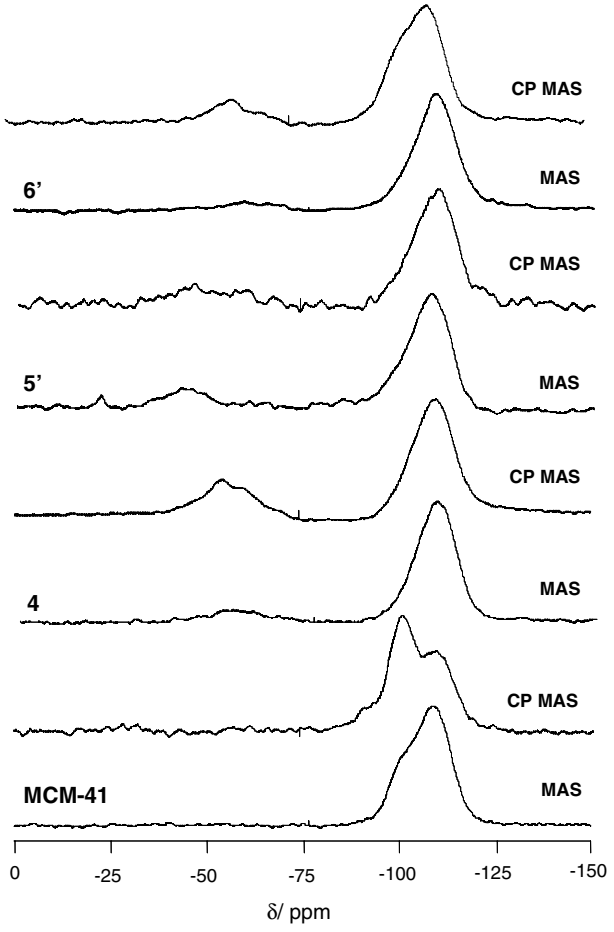

Fig. 3. ^{29}Si MAS and CP MAS NMR spectra of MCM-41, MCM-41-L (**4**), MCM-41-L/Mn(acac)$_2$ (**5′**), and MCM-41-L/VO(acac) (**6′**).

suggest that the complexes were successfully supported on the internal surfaces of the mesoporous silica hosts.

Fig. 3 shows the ^{29}Si MAS and CP MAS NMR spectra for pristine calcined MCM-41, the MCM-41-L (**4**), and the derivatised materials **5**′ and **6**′. Unmodified MCM-41 displays two broad convoluted resonances in the ^{29}Si CP MAS NMR spectrum at −109.2 and −100.8 ppm, assigned, respectively, to Q^4 and Q^3 species of the silica framework [$Q^n = Si(OSi)_n(OH)_{4-n}$]. A weak shoulder is also observed at $\delta = -93.8$ for the Q^2species. The Q^3 sites are associated with the single silanols Si—OH (including hydrogen-bonded silanols), and the Q^2 sites correspond to the geminal silanols. Grafting of the triethoxysilane ligand Ph–DAB–$(CH_2)_3Si(OEt)_3$(**1a**) into MCM-41 reduces the Q^3 and Q^2 resonances owing to the silylation of the surface and, concomitantly, increases the Q^4 resonance. This is consistent with esterification of the isolated silanol groups by nucleophilic substitution at the silicon atom in the organic compounds. The ^{29}Si CP MAS NMR spectrum of **4** display two signals at $\delta = -54.8$, −59.4 ppm and a weak, broad signal at $\delta = -69.0$ ppm, assigned to T^1, T^2 and T^3 organosilica species [$T^m = RSi(OSi)_m(OH)_{3-m}$], respectively, whereas the Q species only present a peak at −108.3 ppm.

The ^{29}Si MAS and CP MAS NMR spectra (Fig. 3) present a significant decrease of the signal to noise ratio. These observations can be related with the presence of paramagnetic nuclei in the materials. The ^{29}Si NMR spectra for materials **5** and **6** are similar to those of **5**′ and **6**′. These results show that for both post-synthesis modification techniques, the organosilanes reacted covalently with the silica surface.

The ^{13}C CP MAS NMR of the functionalised material **4** (not shown) is very similar to that of the free ligand **1a**, in agreement with previous results [14,19]. A decrease in the intensity of the resonances of the SiO–CH_2CH_3 group at 16.5 ppm (CH_3) and 58 ppm (CH_2) is observed since the binding of the ligand to the surface of the host material takes place by the hydrolysis of such groups. The quality of the spectra of the metal containing materials **5**, **5**′ and **6**, **6**′ is poor as a result of the paramagnetism of the complexes, but the position of the peaks can be determined. Thus, for materials **5**′ and **6**′ the peaks observed in the range 0–75 ppm can be assigned to the CH_2 and CH_3 carbons of the propyl chain of the ligand **1a**. In particular, in material **6**′ it is possible to assign some peaks, namely those at 9.6 ($SiCH_2$), 127.9 (phenyl-C), and 192.3 ppm (C═O). The signals observed at around 100 ppm can be assigned to the acac ligand. A similar assignment can be carried out for materials **5** and **6**.

3.2.1. Magnetic properties

Magnetisation measurements were carried out in powder samples of non-supported complexes [$Mn(acac)_2$ {Ph–DAB–$(CH_2)_3Si(OEt)_3$}] (**2a**) and [VO(acac){Ph–DAB–$(CH_2)_3Si(OEt)_3$}]Cl (**3a**), as well as in the materials MCM-41/$Mn(acac)_2$[Ph–DAB–$(CH_2)_3Si(OEt)_3$] (**5**), MCM-41-L/$Mn(acac)_2$ (**5**′), MCM-41/VO(acac)[Ph–DAB–$(CH_2)_3Si(OEt)_3$] (**6**), and MCM-41-L/VO(acac) (**6**′). The analysis of the data using the spin-Hamiltonian model showed that in all Mn based materials (Fig. 4), manganese core is in oxidation state II, with a spin 5/2, showing a higher local symmetry than in the starting reagent $Mn(acac)_3$, which displays local tetragonal symmetry (Jahn–Teller distortion) and spin 2. Mn concentrations obtained from the fitting procedure were 0.63% and 2.91% for materials **5** and **5**′, respectively, in good agreement with elemental analysis results (0.7 and 2.9 wt% for **5** and **5**′, respectively).

In the V(IV)-based materials (Fig. 5), with spin 1/2, such as in $VO(acac)_2$, it is not possible to extract unambiguous information on the local symmetry of vanadium atoms from the fitting procedure. Vanadium concentrations

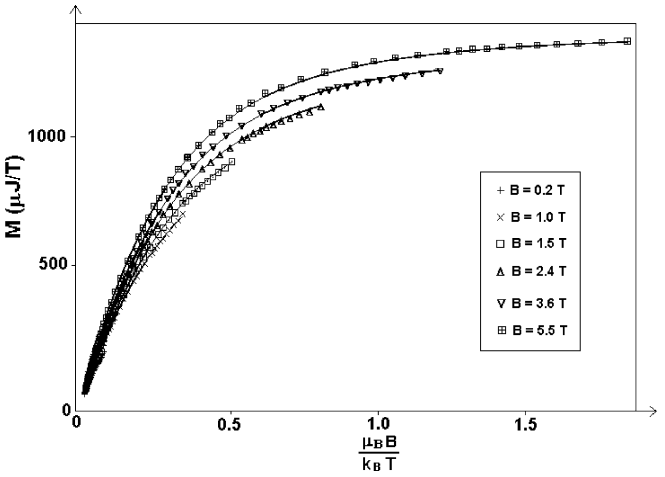

Fig. 4. Magnetisation of [$Mn(acac)_2$L] (**2**) plotted against $\mu_B B/k_B T$ collected at six different magnetic applied fields, between 2 and 200 K, after subtraction of the diamagnetic fraction. The solid lines correspond to least square fitting with the spin-Hamiltonian model [28].

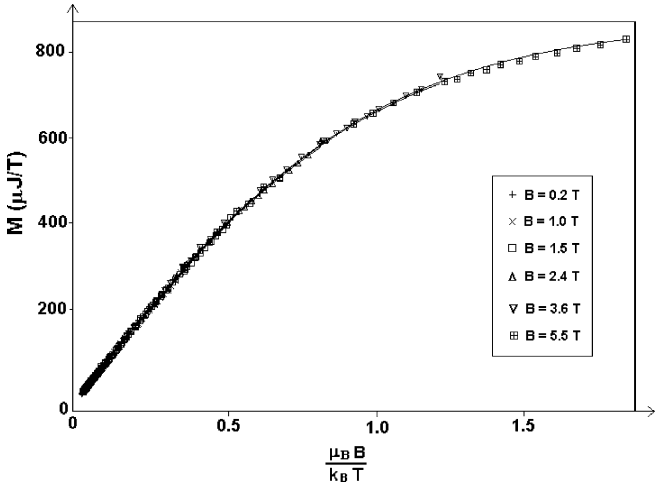

Fig. 5. Magnetisation of [VO(acac)L]Cl (**3**) plotted against $\mu_B B/k_B T$ collected at six different magnetic applied fields, between 2 and 200 K, after subtraction of the diamagnetic fraction. The solid lines correspond to least square fitting with the spin-Hamiltonian model [28].

obtained from the fitting procedure were 0.93% and 2.06% for **6** and **6′**, respectively, in reasonably good agreement with elemental analysis results (0.8 and 2.4 wt% for **6** and **6′**, respectively). The discrepancies observed for the concentration values may be related to the presence of adsorbed molecular oxygen, whose influence is significant for samples with small total magnetic moment. A series of measurements with highly diluted samples (very low concentration of the magnetic moments) are under progress in order to confirm the zero-field splitting parameters obtained, avoiding the presence of surface adsorbed molecular oxygen.

Results from DFT calculations for complexes **2b** and **3b** are in agreement with the findings described, predicting the spin density to lie essentially on the metal centres.

3.2.2. Catalysis

The manganese-containing materials, **2a**, **5** and **5′** were tested as catalysts in the epoxidation of *cis*-cyclooctene using *tert*-butyl hydroperoxide (*t*-BuOOH) as oxygen donor, at 328 K. The reaction is very sluggish without catalyst or in the presence of MCM-41-L (**4**), giving a maximum of 5% conversion after 24 h reaction. In the presence of **2a**, **5** or **5′**, 21–27% conversion is achieved at 24 h, under similar reaction conditions (Fig. 6a). The kinetic profiles obtained for these three catalysts are practically coincident, and they give quite similar initial turnover frequencies (TOF = 1–6 $mol \cdot mol_{Mn}^{-1} \cdot h^{-1}$, Table 3). In all cases, as cyclooctene conversion increases selectivity to 1,2-epoxycyclooctane decreases significantly (drops to 50% as conversion tends to 30%) in detriment of the formation of the corresponding 1,2-diol as the by-product (Fig. 6b). ICP–AES of the solids recovered after the reaction with **5** and **5′** (by filtration, washing with *n*-hexane and drying at room temperature) indicated no measurable loss of Mn. The catalytic activity of **2a**, **5** and **5′** can be compared with that of a $[MoO_2Cl_2L]$ complex (MoL) with the same bidentate 1,4-diazabutadiene ligand (L=RN=C(Ph)–C(Ph)=NR, R=$(CH_2)_3Si(OEt)_3$) supported on MCM-41 (denoted MoL–MCM-41) using a similar grafting procedure [14]. A comparative study of the catalytic activity of **2a** and **5** for cyclooctene epoxidation with that of MoL and MoL–MCM-41, respectively, shows that the Mn catalysts are less efficient than the Mo ones, under similar reaction conditions. For **2a** and MoL TOF (calculated at 1 h reaction) is 2 and 15 $mol\ mol_M^{-1}\ h^{-1}$ and conversion after 24 h is 22% and 56%, respectively, while for the MCM-41-supported complexes, **5** and MoL–MCM-41, TOF is 6 and 13 $mol\ mol_M^{-1}\ h^{-1}$ (M = Mn, Mo) and conversion after 24 h is 22% and 65%, respectively. On the other hand, the Mo catalysts are more selective to the epoxide (100% at ca. 25% conversion) than the Mn ones (ca. 55% at ca. 25% conversion).

Table 3
Epoxidation of cyclooctene with *t*-BuOOH, in the presence of the transition metal catalysts, at 328 K

Catalyst	Initial activity [$mol\ mol_M^{-1} h^{-1}$][a]	Conversion[b] (%)	Selectivity[c] (%)
2a	3	22	59
5	6	22	62
5′	1	27	55
3a	63	73	93
6(run 1)	148	61	98
6(run 2)	23	61	98
6(run 3)	19	60	98
6′(run 1)	150	83	98
6′(run 2)	18	81	100
6′(run 3)	18	81	100

[a] Turnover frequency calculated at ca. 15 min.
[b] Cyclooctene conversion after 24 h.
[c] Selectivity to epoxide at 24 h.

The vanadium materials, **3a**, **6** and **6′** were also tested as catalysts in the epoxidation of cyclooctene with *t*-BuOOH, at 328 K. 1,2-Epoxycyclooctane is the main reaction product formed in more than 98% selectivity at 61% and 83% conversion (at 24 h reaction) in the presence of **6** and **6′**, respectively (Fig. 6b). These results are better than those obtained for the Mn catalysts prepared in the present work,

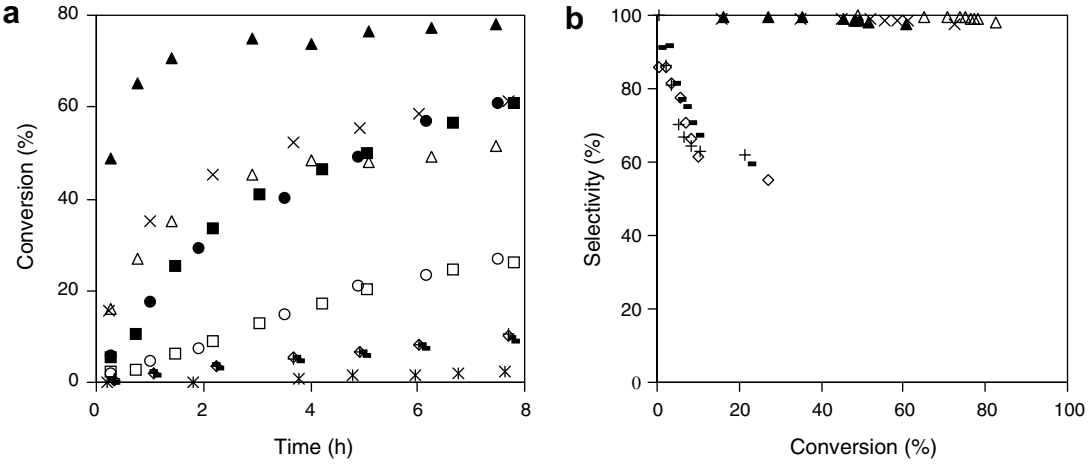

Fig. 6. Kinetic profiles: cyclooctene conversion (a) and selectivity to epoxide versus conversion (b) in the presence of compounds **4** (*), **2a** (−), **5** (+), **5′** (◇), **3a** (×), **6** (open symbols: (△) – first run; (□) – reused once; (○) – reused twice) and **6′** (solid symbols used for **6**), using *t*-BuOOH.

and than those reported in the literature for MoL and MoL–MCM-41, under similar reaction conditions: TOF calculated at 1 h is greater than 100 mol mol_V^{-1} h^{-1} for **6** and **6′**, and equals 35 mol mol_V^{-1} h^{-1} for **3a**, compared to 13 and 15 mol mol_{Mo}^{-1} h^{-1} for MoL–MCM-41 and MoL, respectively [14].

The initial TOF is practically the same for **6** and **6′** (148 and 150 mol mol_V^{-1} h^{-1}, respectively, Table 3). After ca. 15 min, the reaction becomes faster in the presence of **6′** than of **6**, most likely due to the higher metal loading of the former (Fig. 6a). In the case of the unsupported complex **3a**, TOF is significantly lower (63 mol mol_V^{-1} h^{-1}) than that of the supported catalysts **6** and **6′**. This somewhat contrasts with the Mn catalysts in that the unsupported Mn complex **2a** possessed similar catalytic activity to that of the supported catalysts **5** and **5′**. Possibly, partial catalyst deactivation of **3a** occurs to a relatively large extent, under the applied oxidising conditions.

The catalyst stability of **6** and **6′** was examined by recycling the recovered solids (filtered, washed with *n*-hexane and dried at room temperature). Partial loss of catalytic activity is observed mainly from the first to the second reaction run (Table 3). Despite the lower initial reaction rate, after 24 h reaction, the conversion is practically the same as that achieved in the first run. These results may be due to changes in the nature of the active species and/or catalyst deactivation. Leaching tests were performed by filtering the reaction mixture at ca. 15 min to separate the solid at the reaction temperature and leaving the solution to react further. After 3 h, the reaction without the solid catalyst proceeded to roughly the same extent as when filtration was not performed (conversion varied less than 5% of that obtained without filtration). ICP–AES of the recovered solids showed no major change of the vanadium content in the case of **6**. It is possible that small catalyst particles were not separated by the sintered glass filter used for the leaching experiments. However, changes in the nature of the surface metal species under the applied oxidising conditions cannot be ruled out. These results are comparable to that reported in the literature for MoL–MCM-41, in that no measurable metal leaching is observed [14]. In the case of **6′**, the V content decreased 36%, suggesting that for this material loss of activity in consecutive runs is, at least in part, attributed to metal leaching under the applied reaction conditions.

4. Conclusions

The present work has revealed that (a) reaction of $[Mn^{III}(acac)_3]$ and $[V^{IV}O(acac)_2]$ with Ph–DAB–$(CH_2)_3R$ [R = $Si(OEt)_3$; H] (L) in methanol leads to complexes of the type $[Mn^{II}(acac)_2L]$ and $[V^{IV}O(acac)L]Cl$. In the manganese case, the addition of the neutral bidentate ligand facilitates the reduction of Mn(III) to Mn(II) [33]; (b) the 1,4-diazabutadiene ligand bearing triethoxysilyl groups is useful for the preparation of catalytically active manganese(II) and oxovanadium(IV) complexes that can be easily heterogenised on silica supports by covalent bonding. Similar materials were synthesised by the tethering method, by linking the bidentate ligand to the silica surface through stable covalent Si—O—Si bonds, and further reaction with $[Mn(acac)_3]$ and $[VO(acac)_2]$. A higher metal loading was achieved by this method, and the mesoporous regularity was not lost, but the channels seem to be significantly blocked.

The catalytic performance of the unsupported and MCM-41-supported complexes has been investigated in the oxidation of *cis*-cyclooctene with *t*-BuOOH. The vanadium catalysts were more active and selective epoxidation catalysts than the corresponding Mn materials, and than the unsupported and MCM-41-supported molybdenum complexes bearing the same L ligand reported in the literature [14]. In the case of the Mn catalysts epoxide selectivity decreases significantly with conversion, and the corresponding 1,2-diol is formed. While the grafting procedure led to lower vanadium content than the tethering method, the grafted material is more stable towards metal leaching, which is an important issue for practical application of heterogeneous catalysts. However, partial loss of catalytic activity in consecutive reaction runs was observed for tethered and grafted catalysts, suggesting that other deactivation phenomena are involved (possibly, changes in the nature of the surface metal species).

Acknowledgments

The authors are grateful to POCI 2010, FEDER and FCT for financial support (POCI/CTM/55648/2004, POCI/QUI/58925/2004). CDN (SFRH/BPD/27344/2006) and PDV (SFRH/BPD/28149/2006) thank FCT for research grants.

References

[1] Y. Iwasawa, in: Y. Iwasawa, D. Riedel (Ed.), Tailored Metal Catalysts, Dordrecht, 1986, pp. 1–85.
[2] U. Deschler, P. Kleinschmit, P. Panster, Angew. Chem., Int. Ed. Engl. 25 (1986) 236.
[3] C.T. Kresge, M.E. Leonowicz, W.J. Roth, J.C. Vartuli, J.S. Beck, Nature 359 (1992) 710.
[4] J.S. Beck, J.C. Vartuli, W.J. Roth, M.E. Leonowicz, C.T. Kresge, K.D. Schmitt, C.T.-W. Chu, D.H. Olson, E.W. Sheppard, S.B. McCullen, J.B. Higgins, J.L. Schlenker, J. Am. Chem. Soc. 114 (1992) 10834.
[5] J.Y. Ying, C.P. Mehnert, M.S. Wong, Angew. Chem., Int. Ed. 38 (1999) 56.
[6] C.D. Nunes, A.A. Valente, M. Pillinger, A.C. Fernandes, C.C. Romão, J. Rocha, I.S. Gonçalves, J. Mater. Chem.12 (2002) 1735; C.D. Nunes, A.A. Valente, M. Pillinger, J. Rocha, I.S. Gonçalves, Chem. Eur. J. 9 (2003) 4380.
[7] C.D. Nunes, M. Pillinger, A.A. Valente, I.S. Gonçalves, J. Rocha, P. Ferreira, F.E. Kühn, Eur. J. Inorg. Chem. (2002) 1100.
[8] M. Pillinger, C.D. Nunes, P.D. Vaz, A.A. Valente, I.S. Gonçalves, P.J.A. Ribeiro-Claro, J. Rocha, L.D. Carlos, F.E. Kühn, Phys. Chem. Chem. Phys. 4 (2002) 3098.
[9] M.H. Valkenberg, W.F. Hölderich, Catal. Rev. 44 (2002) 321.
[10] D.M. Ford, E.E. Simanek, D.F. Shantz, Nanotechnology 16 (2005) S458.

[11] M. Jia, W.R. Thiel, Chem. Commun. (2002) 2392;
M. Jia, A. Seifert, W.R. Thiel, Chem. Mater. 15 (2003) 2174;
M. Jia, A. Seifert, W.R. Thiel, J. Catal. 221 (2004) 319;
M. Jia, A. Seifert, M. Berger, H. Giegengack, S. Schulze, W.R. Thiel, Chem. Mater. 16 (2004) 877.
[12] P. Ferreira, I.S. Gonçalves, F.E. Kühn, A.D. Lopes, M.A. Martins, M. Pillinger, A. Pina, J. Rocha, C.C. Romão, A.M. Santos, T.M. Santos, A.A. Valente, Eur. J. Inorg. Chem. (2000) 2263.
[13] S. Gago, Y. Zhang, A.M. Santos, K. Köhler, F.E. Kühn, J.A. Fernandes, M. Pillinger, A.A. Valente, T.M. Santos, P.J.A. Ribeiro-Claro, I.S. Gonçalves, Micropor. Mesopor. Mater. 76 (2004) 131;
S.M. Bruno, J.A. Fernandes, L.S. Martins, I.S. Gonçalves, M. Pillinger, P. Ribeiro-Claro, J. Rocha, A.A. Valente, Catal. Today 114 (2006) 263.
[14] C.D. Nunes, M. Pillinger, A.A. Valente, J. Rocha, A.D. Lopes, I.S. Gonçalves, Eur. J. Inorg. Chem. (2003) 3870;
C.D. Nunes, M. Pillinger, A.A. Valente, A.D. Lopes, I.S. Gonçalves, Inorg. Chem. Commun. 6 (2003) 1228.
[15] K. Wieghardt, Angew. Chem., Int. Ed. Engl. 28 (1989) 1153;
V.L. Pecoraro (Ed.), Manganese Redox Enzymes, VCH, New York, 1992;
G.C. Dismukes, Chem. Rev. 96 (1996) 2909.
[16] J. Inorg. Biochem. 80 (2000) (special issue dedicated to biological aspects of vanadium).
[17] Z. Luan, J. Xu, L. Kevan, Chem. Mater. 10 (1998) 3699.
[18] P. Sutra, D. Brunel, Chem. Commun. (1996) 2485.
[19] J. Gimenez, C.D. Nunes, P.D. Vaz, A.A. Valente, P. Ferreira, M.J. Calhorda, J. Mol. Catal. A: Chem. 256 (2006) 90.
[20] R.G. Charles, Inorg. Syn. 6 (1960) 164.
[21] M. Bhattacharjee, J. Chem. Res. (S) (1992) 415.
[22] R.G. Parr, W. Yang, Density Functional Theory of Atoms and Molecules, University Press, Oxford, New York, 1989.
[23] M.J. Frisch, G.W. Trucks, H.B. Schlegel, G.E. Scuseria, M.A. Robb, J.R. Cheeseman, J.A. Montgomery Jr., T. Vreven, K.N. Kudin, J.C. Burant, J.M. Millam, S.S. Iyengar, J. Tomasi, V. Barone, B. Mennucci, M. Cossi, G. Scalmani, N. Rega, G.A. Petersson, H. Nakatsuji, M. Hada, M. Ehara, K. Toyota, R. Fukuda, J. Hasegawa, M. Ishida, T. Nakajima, Y. Honda, O. Kitao, H. Nakai, M. Klene, X. Li, J.E. Knox, H.P. Hratchian, J.B. Cross, V. Bakken, C. Adamo, J. Jaramillo, R. Gomperts, R.E. Stratmann, O. Yazyev, A.J. Austin, R. Cammi, C. Pomelli, J.W. Ochterski, P.Y. Ayala, K. Morokuma, G.A. Voth, P. Salvador, J.J. Dannenberg, V.G. Zakrzewski, S. Dapprich, A.D. Daniels, M.C. Strain, O. Farkas, D.K. Malick, A.D. Rabuck, K. Raghavachari, J.B. Foresman, J.V. Ortiz, Q. Cui, A.G. Baboul, S. Clifford, J. Cioslowski, B.B. Stefanov, G. Liu, A. Liashenko, P. Piskorz, I. Komaromi, R.L. Martin, D.J. Fox, T. Keith, M.A. Al-Laham, C.Y. Peng, A. Nanayakkara, M. Challacombe, P.M.W. Gill, B. Johnson, W. Chen, M.W. Wong, C. Gonzalez, J.A. Pople, Gaussian 03, Revision B.04, Gaussian, Inc., Wallingford, CT, 2004.
[24] F.H. Allen, Acta Crystallogr. B58 (2002) 380.
[25] A.D. Becke, J. Chem. Phys. 98 (1993) 5648;
B. Miehlich, A. Savin, H. Stoll, H. Preuss, Chem. Phys. Lett. 157 (1989) 200;
C. Lee, W. Yang, G. Parr, Phys. Rev. B. 37 (1988) 785.
[26] T.H. Dunning Jr., P.J. Hay, in: H.F. Schaefer (Ed.), Modern Theoretical Chemistry, vol. 3, Plenum, New York, 1976, pp. 1–28;
P.J. Hay, W.R. Wadt, J. Chem. Phys. 82 (1985) 270;
W.R. Wadt, P.J. Hay, J. Chem. Phys. 82 (1985) 284;
P.J. Hay, W.R. Wadt, J. Chem. Phys. 82 (1985) 299.
[27] A.D. McClean, G.S. Chandler, J. Chem. Phys. 72 (1980) 5639;
R. Krishnan, J.S. Binkley, R. Seeger, J.A. Pople, J. Chem. Phys. 72 (1980) 650;
A.J.H. Wachters, J. Chem. Phys. 52 (1970) 1033;
P.J. Hay, J. Chem. Phys. 66 (1977) 4377;
K. Raghavachari, G.W. Trucks, J. Chem. Phys. 91 (1989) 1062;
R.C. Binning, L.A. Curtiss, J. Chem. Phys. 103 (1995) 6104;
M.P. McGrath, L. Radom, J. Chem. Phys. 94 (1991) 511.
[28] E.P. Day, Methods Enzymol. 227 (1993) 437.
[29] A.A. Romero, M.D. Alba, W. Zhou, J. Klinowski, J. Phys. Chem. B 101 (1997) 5294;
J. Xu, Z. Luan, H. He, W. Zhou, L. Kevan, Chem. Mater. 10 (1998) 3690.
[30] B. Marler, U. Oberhagemann, S. Voltmann, H. Gies, Micropor. Mater. 6 (1996) 375;
W. Hammond, E. Prouzet, S.D. Mahanti, T.J. Pinnavaia, Micropor. Mesopor. Mater. 27 (1999) 19.
[31] S.J. Gregg, K.S.W. Sing, Adsorption, Surface Area and Porosity, second ed., Academic Press, London, 1982.
[32] M.D. Alba, A. Becerro, J. Klinowski, J. Chem. Soc., Faraday Trans. 92 (1996) 849.
[33] R. van Gorkum, E. Bouwman, J. Reedijk, Inorg. Chem. 43 (2004) 2456.